Parasitology Research (2023) 122:979–988
https://doi.org/10.1007/s00436-023-07801-x

RESEARCH

Antimalarial activity assay of artesunate-3-chloro-4(4-chlorophenoxy) aniline in vitro and in mice models

Milka Wambui Waithera[1,2] · Martin Wekesa Sifuna[1] · Daniel Wainaina Kariuki[2] · Johnson Kang'ethe Kinyua[2] · Francis Thuo Kimani[3] · Joseph Kang'ethe Ng'ang'a[2] · Masahiro Takei[1]

Received: 7 August 2022 / Accepted: 20 February 2023 / Published online: 2 March 2023

Abstract

The global spread of multi-drug resistant *P. falciparum*, *P. vivax*, and *P. malariae* strains and absence of long-term effective vaccine makes chemotherapy the mainstay of malaria control strategies in endemic settings. The Mossman's assay and the Organization for Economic Co-operation and Development (OECD), 2001 guideline 423, were used to determine the cytotoxicity and acute oral toxicity of a novel hybrid drug, artesunate-3-Chloro-4(4-chlorophenoxy) aniline (ATSA), in vitro and in vivo, respectively. A modified Desjardins method was used to screen for antiplasmodial activity using *P. falciparum* ($3D_7$ and W_2) strains in vitro. The Peter's 4-day suppressive tests (4DTs) was used to evaluate the in vivo antimalaria activity using *P. berghei* ANKA strain, lumefantrine resistant (LuR), and piperaquine resistant (PQR) *P. berghei* lines. *In silico* prediction of absorption, distribution, metabolism, excretion, and toxicity (ADMET) profiles was assayed using PreADMET online prediction tool. The reference drug in all experiments was artesunate (ATS). Statistical significance between ATSA's activities in treated and control mice was evaluated by one-way analysis of variance (ANOVA). Results show that inhibitory concentrations-50 (IC_{50}) of ATSA is 11.47 ± 1.3 ($3D_7$) and 1.45 ± 0.26 (W_2) against 4.66 ± 0.93 ($3D_7$) and 0.60 ± 0.15 (W_2) ng/ml of ATS with a selective index of 2180.91($3D_7$) and a therapeutic index (TI) of > 71). No mortalities were observed in acute oral toxicity assays and mean weight differences for test and controls were statistically insignificant ($P > 0.05$). The in vivo activity of ATSA was above 40% with effective dosage-50 (ED_{50}) of 4.211, 2.601, and 3.875 mg/kg body weight against *P. berghei ANKA*, LuR, and PQR lines, respectively. The difference between treated and control mice was statistically significant ($P < 0.05$). ATSA has high intestinal absorption (HIA) > 95% and has medium human ether-a-go-go related gene (hERG) K^+ channel inhibition risks. Preclinical and clinical studies on ATSA are recommended to evaluate its value in developing novel drugs for future management of multi-drug resistant malaria parasites.

Keywords Antimalaria · Artesunate-3-chloro-4-(4-chlorophenoxy) aniline · Hybrid drugs · ADMET profiles

Introduction

Malaria is still a global health burden (Joseph et al. 2019; Beteck et al. 2014). An estimated 241 M cases and 627,000 deaths were reported in 2020 with the highest disease burden occurring in the sub-Saharan Africa (Cravo 2022; Nghochuzie et al. 2020). The major parasite species responsible for global malaria incidences are *P. vivax;* the most wide spread (Angrisano and Robinson 2022) and *P. falciparum* (Hermansyah et al. 2017) the most virulent (Tachibana et al. 2022). Acquired immunity (Joseph et al. 2019) which develops after a few episodes of parasite infections is short-lived (Horata et al. 2017). Vaccine development to boost host immunity, remains elusive hence chemotherapy is the mainstay of

Handling Editor: Una Ryan

✉ Martin Wekesa Sifuna
sifuna@chiba-u.jp

[1] Department of Mechanical Engineering, Graduate School of Science and Engineering, Chiba University, 1-33, Inage-Ku, Chiba-Shi, Chiba 263-8522, Japan

[2] Department of Biochemistry, Jomo Kenyatta University of Agriculture and Technology, P.O Box 62000-00200, Nairobi, Kenya

[3] Centre for Biotechnology Research and Development, Kenya Medical Research Institute, P.O Box, Nairobi 54840-00200, Kenya

malaria control efforts (Dhanawat et al. 2009). Hybrid therapy is a recent approach which involves linking two compounds with individual mechanisms of action into a single molecule (Muregi and Ishih 2010). The resultant hybrid drugs exhibit enhanced chemo-therapeutic profiles (Meunier 2008) such as reduced drug toxicity, increased therapeutic outcome, and improved dosage compliancy (Lombard et al. 2013; Nilsen et al. 2014). They also display high parasite selectivity (Sharma et al. 2014) due to synergistic output of hybridized molecules. Development of resistant parasites is also circumvented or delayed since individual molecules target the parasite using different modes of action (Muregi and Ishih 2010; Nilsen et al. 2014).

Various antimalarial drugs have been developed since the onset of hybridization. They include 4-aminoquinoline-pyrimidine that exhibited enhanced therapeutic outcome to both sensitive and resistant malaria parasites (Meunier 2008).

PA1103-SAR116242 showed improved antimalarial potency against CQ resistant and pyrimethamine resistant malaria strains; it acts by inhibiting hemozoin bio-crystallization (aminoquinoline moiety) and alkylating heme molecules (Meunier 2008). Trioxaquine comprising artesunate and 4,7-dichloroquinoline manifested superior antimalarial efficacy in treatment of cerebral malaria compared to precursors separately (Odhiambo et al. 2017). 4-Aminoquinolone-pyrimidine-derived hybrids also manifested higher efficacies in *P. falciparum* sensitive (D_6) and resistant (W_2) clones in vitro as well as in vivo in *P. berghei* parasites with wide safety margins compared to chloroquine (Manohar et al. 2012). Mefloquine-artesunate hybrid (MEFAS) derived from hybridization of mefloquine and artesunate gave improved potency compared to single molecules in vitro on *P. falciparum* W_2 and $3D_7$ clones and in vivo on *P. berghei* NK65 strain (Varotti et al. 2008).

Malaria control is extremely hampered by existing multi-drug resistant *Plasmodium falciparum*, *Plasmodium vivax*, and *Plasmodium malariae* strains (Feng et al. 2020). Since the rapidly growing malaria parasites portray an exacerbated demand for lipids (Sifuna et al. 2019), type 2 fatty acid biosynthesis pathway offers an excellent target for antimalarial drugs. Inhibition of a vital *P. falciparum* enzyme; enoyl acyl carrier protein reductase (Pf. EACP) which catalyzes a NADH-dependent reduction of *trans*-2-enoyl-ACP to acyl-ACP, halts parasite survival (Sifuna et al. 2019). In this study, artesunate-3-chloro-4-(4-chlorophenoxy) aniline(ATSA) hybrid molecule was synthesized via covalent linkage of artesunate (ATS) and 3-chloro-4-(4-chlorophenoxy)aniline (ANI) under the concept of covalent biotherapy (Muregi and Ishih 2010). Toxicity assays of ATSA was determined by Mossman's and the Organization for Economic Co-operation and Development (OECD) 423 protocols. Antimalarial activities were determined in vitro using *P. falciparum* ($3D_7$) and (W_2) and in mice using *P. berghei* ANKA and *P. berghei* lumefantrine resistant (LuR) and piperaquine resistant (PQR) parasite lines. The absorption, distribution, metabolism, excretion, and toxicity (ADMET) profiles were predicted *in silico* using the Pre-ADMET online tool. Artesunate (ATS) was used as a reference drug.

Experimental setup, methods, and conditions

Experimental site

This study was laboratory-based and all experiments were conducted at the malaria unit of the Centre for Biotechnology, Research and Development (CBRD), and the Centre for Traditional Medicine and Drug Research (CTMDR) both of Kenya Medical Research Institute (KEMRI) Headquarters, Mbagathi, Nairobi, Kenya.

Experimental animals

Randomly bred Swiss albino mice, 5 to 6 weeks old, same sex weighing 20 ± 2 g were maintained in an animal house experimental room in standard polypropylene (hard plastic) cages. The mice were placed in groups of three or five (separate male and female), clearly labeled with experimental details and fed on commercial rodent food and water ad libitum. Good Laboratory Practice and the KEMRI's Animal Care and Use Committee (ACUC) standards and regulations were strictly adhered to hence minimizing animal suffering during all the assays. At the end of the experiments, both dead and moribund mice were euthanized using sodium pentobarbital (150 mg/kg), placed in biohazard disposable bags and autoclaved at 121 °C for 15 min to reduce environmental contamination during incineration.

Malaria parasites, Vero cells, and test drugs

Cryopreserved *P. falciparum,* the chloroquine (CQ) sensitive $3D_7$ and CQ resistant, W_2, *P. berghei* ANKA strain, *P. berghei* lumefantrine resistant (LuR), *P. berghei* piperaquine resistant (PQR), and Vero cell lines used in the assays were obtained from the KEMRI-CTMDR laboratory. To revive the cryopreserved *P. berghei* parasites, their suspensions were initially thawed, centrifuged to remove the cryopreservative and injected into three groups (*P. berghei* ANKA, LuR, and PQR) of two mice each using a needle of size $26G \times 5/8''$ through the intraperitoneal route. The parasites were passaged on a weekly basis into naive mice to resuscitate their virulence. These infected mice served as donors for setting the standard 4-day suppressive tests (4-DT) and curative tests after establishing a steady state

parasitemia. Artesunate (ATS) was purchased from Sigma-Aldrich®, India. The hybrid drug (ATSA) was synthesized by covalently linking its precursors ATS and ANI through a sequential coupling solvent extraction process as summarized in Fig. 1. Briefly, 0.5 mmol of ATS was dissolved in dichloromethane (DCM) of volume $v = 5$ ml. 1-Ethyl-3-(3-dimethylaminopropyl) carbodiimide hydro-chloride (EDC) (1.5 eq), 1-hydroxy-benzotriazole (HOBt) (1.5 eq), and diisopropylethylamine (DIPEA) (3.0 eq) were then added and the whole mixture stirred at 0 °C in a round bottomed flask. To this mixture was added a solution of ANI (1.0 mmol) dissolved in 5 ml of DCM dropwise and the reaction stirred at room temperature overnight. The mixture was the quenched off with saturated $NaHCO_3$, the organic phase separated and the aqueous phase back extracted with methylene chloride. Combined organic layers were dried using anhydrous magnesium sulfate ($MgSO_4$), filtered and the solvent removed in vacuo.

Toxicity assays

Cytotoxicity assays

Vero E6 cell line was used to screen for the cytotoxicity of ATSA using the Mosmann, 3-(4,5-dimethylthiazol-2-yl)-2,5-diphenyltetra-zolium bromide (MTT) cell viability assay. Prior to the assay, the trypan blue exclusion method was used to determine the cell density using an inverted microscope (A. Kruss Optronic, Germany) at × 400 magnification. Briefly, 100 µl of cell suspension at a density of 2×10^4 was seeded into 96-well flat-bottomed microtiter plates. The culture plates were then incubated at 37 °C with 5% CO_2 for 24 h. Thereafter, 150 µl of the test drugs were added and a triplicate dilution was performed. The plates were again incubated for 24 h before 10 µl of 5 mg/ml MTT solution was added to each well to give a final concentration of 0.5 mg/ml. These plates were incubated for a further 4 h followed by addition of 100 µl dimethyl sulfoxide (DMSO) to dissolve formazan crystals. The absorbance was read at 562 nm/690 nm using a scanning multi-well spectrophotometer (Multi-scan EX Lab-systems). Data was entered in a MICROSOFT EXCEL software and inhibitory concentration that causes death of 50% cells (CC_{50}) determined using Eq. 1 (Mosmann 1983).

$$CC_{50} = \frac{\left(\text{Absorbance}_{562} - \text{Absorbance}_{690}\right)\text{test}}{\left(\text{Absorbance}_{562} - \text{Absorbance}_{690}\right)\text{control}} \times 100 \quad (1)$$

The selective indices (SI) of the drugs were determined by Eq. 2:

$$SI = \frac{CC_{50} \text{ of mammaliancells}}{IC_{50} \text{ of parasitecells}} \quad (2)$$

Acute oral drug toxicity assays

Acute oral toxicity was conducted in accordance with the Organization of Economic Co-operation and Development (OECD 2001) guideline 423 Jonsson et al. 2013. Swiss female albino mice (three mice per group), 7 weeks old and weighing between 20 and 26 g were used. The mice were starved for 3 h, weighed and 200 µl of a single dose of 300 mg/kg body weight (bwt) of freshly prepared solutions of ATSA and ATS given by oral gavage using a stainless-steel feeding cannula. Negative control group received equal volume of distilled water. The mice were then observed continuously for the first 30 min post drug administration and then after 4 h and 24 h for any physical signs of drug intoxication: mortality, gross behavior, body conditions such as tremors, diarrhea, lethargy, salvation, and convulsions. The mice were continuously monitored at intervals of

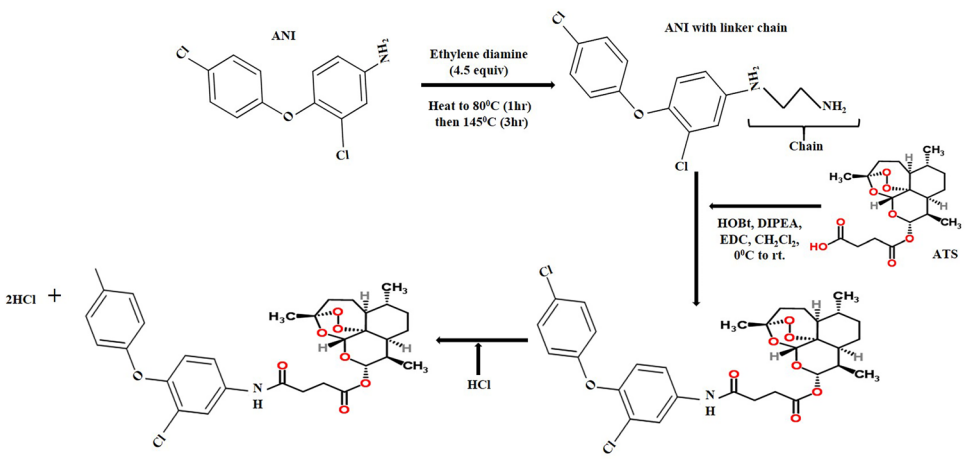

Fig. 1 Hybridization of ATS and ANI to form artesunate-3-chloro-4-(4-chlorophenoxy) aniline (ATSA) hybrid

4 days for 14 days with surviving mice weighed and the weight recorded. Therapeutic index (TI) of test drugs was then determined by Eq. 3:

$$TI = \frac{LD_{50}}{ED_{50}} \quad (3)$$

where LD_{50} is lethal dose which cause death to 50% of the test animals while ED_{50} is the effective dose that suppresses 50% of the parasite (Muller and Milton 2012).

In vitro *antiplasmodial screening assays*

Human malaria parasites were cultured using the method of Trager and Jensen with slight modifications (Trager and Jensen 1976). *P. falciparum* cultures were maintained continuously at 37 °C followed by a 72 h susceptibility tests using radio-labelled [3H] hypoxanthine incorporation semi-automated microdilution assay technique in 96-well microtiter plates. Early-stage parasites, $3D_7$ and W_2, were tested in duplicate. Briefly, 25 µl complete culture medium was added to all wells. Twenty-five microliters of either ATSA or TSA drugs was then added. A serial twofold dilution over a 64-fold concentration range was carried out using a motorized hand diluter. Two hundred microliters of parasitized RBCs at 0.4% parasitemia was then added to test wells. Into some control wells, 200 µl of non-parasitized RBCs was added. The plates were place in an air-tight gas chamber, gassed with 3% CO_2, 5% O_2, and 92% N_2 and incubated for 72 h at 37 °C. Each specific well was then pulsed with 25 µl of culture medium containing 0.5 µCi of [3H] hypoxanthine and the plates incubated for 18 h. The contents of each well was harvested in glass fiber filters, washed several times and radioactivity measured in counts per minute using a liquid scintillator (Khan et al. 2017). The 50% inhibitory concentration (IC_{50}) was obtained by nonlinear probit or regression of percentage growth inhibition for each drug.

In vivo *assays*

Parasite inoculation

Infected red blood cells (iRBCs) was collected into heparinized syringes using a needle whose size was 26G × 5/8 following cardiac puncture of the anesthetized donor mice with increasing parasitemia of between 10 and 15%. The parasitemia was adjusted downwards to approximately 1% using autoclaved phosphate saline with glucose (PSG) buffer. The buffer was initially constituted using 2.696 g disodium hydrogen phosphate, 5 g glucose, 0.156 g hydrated sodium dihydrogen phosphate, and 0.85 g sodium chloride all dissolved in 500 ml double-distilled water, sterilized by autoclaving and stored in the dark at 4 °C. During parasite injection, a mouse was restrained by holding tail ends with one hand while gently but firmly holding the loose skin at the neck and back using the same hand. The mouse was then held in an upright position and 200 µl parasite inoculum injected in the intraperitoneal (*ip*) cavity using the other hand.

Early infection tests

The standard 4-day chemo-suppressive tests (4DTs) were used to assess the percentage reduction in parasitemia in mice injected with *P. berghei* ANKA, LuR, and PQR iRBCs as described by Peters et al. (1975). Briefly, infected mice were distributed randomly into three test dose groups and a negative control group of five mice each. Drug solutions were freshly prepared just before administration by first solubilizing in dimethyl sulfoxide (DMSO) final concentration 1% followed by serial dilution with distilled water to required experimental concentrations. Two hundred microliters of each drug were administered orally to the mice at a time $t = 3$ h, 24 h, 48 h, and 72 h post infection using a stainless steel, 24-gauge feeding cannula (Harvard Apparatus; 25 mm in length, 1.25 mm ball diameter). Negative controls received distilled water. On day 4 (96 h) pi, thin blood smears from mice tail snips were prepared.

Thin smear staining and examination

Thin blood smears were fixed by immersing slides in absolute methanol for 30 s, air-drying, staining with 10% working Geimsa solution for 20 min, washing over running tap water and drying at the extreme edge of the hood (Omwoyo et al. 2014). A drop of immersion oil was placed on the smears and parasites examined using a microscope (OLYMPUS X3) at × 1000 magnification. Parasite load (percentage parasitemia; *PP*) from four random microscope fields was calculated using Eq. 4:

$$PP = \frac{T_{iRBC}}{T_{RBC}} \times 100 \quad (4)$$

where T_{iRBC} is the total number of infected RBCs while T_{RBC} is the total number of RBCs. Percentage parasitemia suppression (*PPS*) (chemo-suppression) was determined using Eq. 5:

$$PPS = \frac{A - B}{A} \times 100 \quad (5)$$

where *A* is the mean parasitemia in negative control group while *B* is the mean parasitemia in test groups.

Curative test

Experimental mice were injected ip with the *P. berghei* ANKA iRBCs and randomized into two test groups and a negative control of five mice each. Smears were made on D_4 post-infection just before start of treatment to confirm infection and determine initial parasitemia. Drug solutions equivalent to ED_{50s} of ATSA obtained in early infection test was administered on D_4, D_5, and D_6. Smears were made on D_7, D_9, D_{11}, and D_{13} to monitor the reduction in parasitemia. Percentage parasitemia was determined as previously described and average percentage suppression (*APS*) of parasitemia determined using Eq. 6:

$$APS = \frac{PD_4}{PD_7} \times 100 \quad (6)$$

where PD_4 is the average % parasitemia before treatment, day 4, while PD_7 is the average % parasitemia after treatment, day 7.

In silico prediction of ADMET profiles

ADMET profiles were predicted using Pre-ADMET online prediction tool. The 2D structures of ATSA and ATS were drawn using an online user interphase Chem-Doodle® drawing tool in Pre-ADMET server and directly submitted for calculation of absorption, distribution, metabolism, and toxicity parameters.

Data analysis

The in vitro data was expressed as mean ± SD while in vivo data was processed in Microsoft® Excel (Microsoft Corp.) data sheet and effective dose fifty (ED_{50}) estimated graphically by linear regression using Statistica 2000 version 5.5. Statistical difference was determined using one-way analysis of variance (ANOVA) where a value of $P < 0.05$ was set as statistically significant.

Results

In vitro *cytotoxicity and antiplasmodial activity*

As shown in Fig. 2, the concentrations capable of causing visible alterations by 50% and thus inhibiting growth of cells (CC_{50}) was 25.015 ± 2.325 µg/ml and 48.945 ± 0.035 µg/ml for ATSA and ATS, respectively. The IC_{50} for ATSA were 11.47 ± 1.3 ng/ml and 1.45 ± 0.11 ng/ml compared to 2.00 ± 0.93 ng/ml and 1.9 ± 0.15 ng/ml for ATSA using (3D7) and (W2), respectively. The selective index (SI_{50}) was 2180.91 for ATSA and 42,475 for ATS using the sensitive $3D_7$ clone.

Acute in vivo *toxicity*

After 14 days, the mean weights of experimental mice in test and control groups ranged between 22.0 mg/kg body weight to 23.75 mg/kg as shown in Table 1. The mean weight difference between the test and control groups was statistically insignificant, $P > 0.05$. Based on these results, the LD_{50}s for ATSA drug was estimated to be > 300 mg/kg bwt.

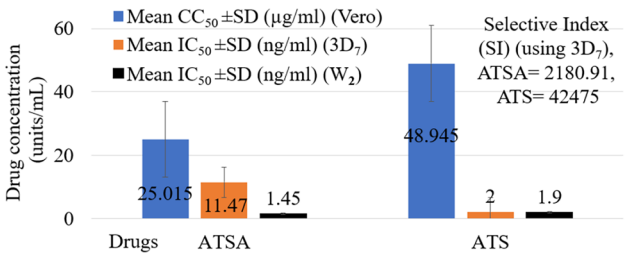

Fig. 2 In vitro cytotoxicity and anti-plasmodial activity

Table 1 Mice weights in acute oral toxicity assay after 300 mg/kg body weight dose

	Group	Mice identity	D1	D5	D9	D14	Mean weight ± SD (mg/kg)
Weights of mice	ATSA	M1	24	22	24	25	23.75 ± 1.26
		M2	24	24	22	25	23.75 ± 1.26
		M3	22	24	22	23	22.75 ± 0.96
	Control	M1	20	24	24	22	22.5 ± 1.91
		M2	20	24	24	22	22.5 ± 1.91
		M3	20	24	24	22	22.5 ± 1.91

In vivo *antimalarial activity assays*

Early infection test

Percentage chemo-suppression of ATSA and ATS were determined in mice using the standard 4DTs against *P. berghei* ANKA, LuR, and PQR parasites. The results demonstrate dose-dependent relationships. In *P. berghei* ANKA, parasite chemo-suppression after a 3.0 mg/kg body weight was 41.47% for ATSA. ATSA suppressed LuR parasites by 63.30% and PQR parasites by 55.66% as shown in Fig. 3. The percentage activities of ATSA in *P. berghei* ANKA, LuR, and PQR compared to the controls were statistically significant $P < 0.05$. The effective dosages capable of decreasing the population of parasites by fifty percent (ED_{50s}) were 4.211 mg/kg/day, 2.601 mg/kg/day, and 3.875 mg/kg/day for ATSA and 2.108 mg/kg/day, 1.883 mg/kg/day, and 0.961 mg/kg/day for ATS against *P. berghei* ANKA, LuR, and PQR parasites,respectively, as shown in Fig. 4.

Curative test

The average percentage chemo-suppression of ATSA in the curative test against *P. berghei* ANKA were determined on D_7 in mice treated for 3 days (D_4 to D_6) with the drug's ED_{50s} value of 4.211 mg/kg/day obtained in the early infection test. The ATSA showed similar inhibitory potential compared to the untreated control and the percentage chemo-suppression of ATSA novel drug was statistically significant $P < 0.05$. Figure 5 indicates the average parasitemia between D_4 and D_{13}. The parasite load decreased gradually till D_7. Beyond D_7, growth of parasites began to increase.

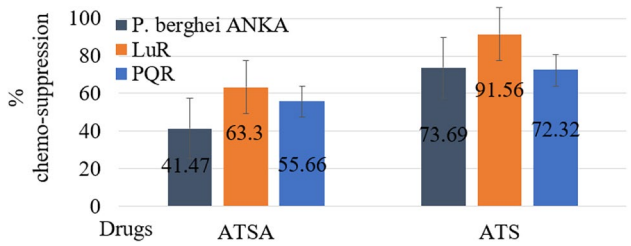

Fig. 3 In vivo percentage parasitemia in early infection test

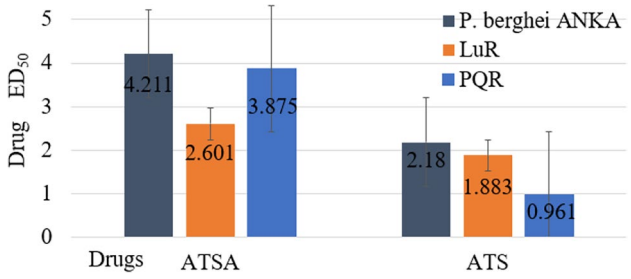

Fig. 4 In vivo effective dosage-50 (ED_{50})

In silico ADMET profiles

Absorption, distribution, metabolism, and toxicity profiles of ATSA with reference ATS were determined *in*

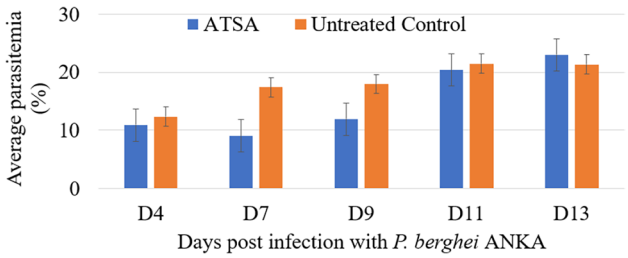

Fig. 5 In vivo activity of ATSA in a curative test

Table 2 ADME and toxicity profiles of ATSA against ATS

Target test	ATSA	ATS
HIA (%)	96.831371	88.675981
Caco-2 (cm/s)	29.8626	13.1902
MDCK (cm/s)	0.0695573	0.344241
P-gp inhibition	Inhibitor	Non-inhibitor
Skin permeability	−2.44849 (cm/h)	−3.77087 (cm/h)
BBB (C_{brain}/C_{blood})	0.355308	0.0112762
PPB (%)	91.507	70.122
CYP2C19 inhibition	Inhibitor	Inhibitor
CYP 2C9 inhibition	Inhibitor	Inhibitor
CYP 2D6 inhibition	Inhibitor	Non
CYP 2D6 substrate	Non	Non
CYP 3A4 inhibition	Inhibitor	Inhibitor
CYP 3A4 substrate	Substrate	Substrate
Ames test	Mutagen	Non-mutagen
Mouse carcinogenicity	Non-carcinogen	Carcinogen
Rat carcinogenicity	Carcinogen	Non-carcinogen
hERG inhibition	Medium-risk	Low-risk
TA 100_10RLI	Non-mutagen	Non-mutagen
TA 100_NA	Non-mutagen	Non-mutagen
TA 1535_10RLI	Non-mutagen	Non-mutagen

HIA human intestinal absorption, *Caco-2* human epithelial adenocarcinoma colorectal cell line, *MDCK* Mandin-Darby canine kidney, *BBB* blood–brain barrier, *PPB* plasma protein binding, *P-gp* P-glycoprotein, *CYP* cytochrome P450 subfamily, *hERG* human either-a-go-go gene, *TA100/1535 S. typhimurium* strain, *RLI* rat liver homogenate, *NA* no metabolic activation

silico, and the results are summarized in Table 2. Most ADMET parameters of the ATSA are similar as those of ATS which indicates the safety of the novel hybrid drug candidate.

Absorption profile

The human intestinal absorption (HIA), permeability to the human epithelial colorectal adenocarcinoma (Caco-2) cells, the Mandin-Darby canine kidney (MDCK) cells, P-glycoprotein (P-gp) inhibition, and skin permeability profiles demonstrate the absorption parameters. The novel drug ATSA shows a slightly higher HIA value, 96.831371% as compared to HIA value of 88.675981% for ATS. ATSA also exhibits a remarkably low permeability to MDCK cells (0.0695573* cm/s) as compared to 0.344241 cm/s for ATS but has high permeability to CaCO-2 cells (29.8626 cm/s) compared to 13.1902 cm/s for ATS.

ATSA inhibits P-gp and has a skin permeability of − 2.53826 cm/h while ATS is a non-inhibitor to P-gp with a skin permeability of − 3.77087 (cm/h), Table 2.

Distribution profile

Brain-blood barrier (BBB) penetration and percentage plasma protein binding (PPB) parameters display distribution patterns of ATSA and ATS. ATSA show a BBB value of 0.355308 compared to 0.0112762 for ATS. The PPB is 91.507% and 70.122% for ATSA and ATS respectively, Table 2

Metabolism profile

Metabolism was determined by screening whether ATSA in comparison with ATS was an inhibitor or a substrate to various members of cytochrome P450 gene (CYP) subfamilies: CYP 2C19 inhibition, CYP 2C9 inhibition, CYP 2D6 inhibition, CYP 3A4 inhibition, CYP 2D6 substrate, and CYP 3A4 substrate using Pre-ADMET predictor. It was found that ATSA is an inhibitor of CYP 2C19, CYP 2C9 and CYP 3A4 and non-substrate to CYP 2D6. ATSA also inhibits CYP 2D6 but it is a substrate for CYP 3A4, Table 2.

Toxicity profile

Toxicity was determined by screening for Ames mutagenicity, carcinogenicity in mouse or rat models and human ether-a-go-go related gene (hERG) potassium ion (K^+) channel inhibition. ATSA shows non-mutagenicity to both TA100 and TA1535 strains similar to ATS. ATSA is carcinogenic to the rat model but not mouse model while ATS is carcinogenic to the mouse model alone. ATSA exhibit medium risks while ATS displays low risk of hERG K^+ channel inhibition, Table 2.

Discussion

The world continues to lose effective antimalarial drugs due to the growing number of multi-drug resistant human malaria parasites. Since malaria continues to cause death mostly to children below the age of 5 years and pregnant women particularly in sub-Saharan Africa, alternative medications efficacious to both sensitive and resistant parasites are in constant need. This study thus evaluated the antimalarial activity, toxicity and *in silico* ADMET profiles of a novel molecule, artesunate-3-chloro-4(4-chlorophenoxy) aniline (ATSA) hybrid. Artesunate (ATS) was used as a standard drug. The in vitro cytotoxicity results revealed that the hybrid drug has a wide safety margin of 2180.91 compared to 42,475 for ATS using the sensitive $3D_7$ strain. No mortalities or significant weight differences occurred between the negative control mice and mice treated with ATSA at 300 mg/kg bwt. The LD_{50} for ATSA was estimated to be > 300 mg/kg with a therapeutic index (TI) > 71. The resultant safety margin was more than 30 times the effective dosage; 4.211 mg/kg/day required to reduce the parasite population by 50% (ED_{50}).

ATSA exerted parasite chemo-suppression to both the sensitive and resistant *P. falciparum* and *P. berghei* parasites, $P > 0.05$. However, the antimalarial activity of ATSA was observed to be less than that of the popular clinically used trioxane drug artesunate. This might have been due to low solubility of the aniline component, which could in turn have affected the overall efficacy of the hybrid antimalarial candidate drug. It is also possible that ANI is a short acting drug and since artesunate is similarly a short acting antimalarial medicine, a decrease in the percentage parasite chemo-suppression for the hybrid was evident. However, the potency of this drug candidate may be enhanced through specific slight modifications of the linker as these have been shown to improve the chemotherapeutic outcome of hybridized drugs (Dambuza et al. 2015). ATSA targets the malaria parasites by two distinct mechanisms, ANI is critical in the FAS-II pathway in plasmodium apicoplasts (Sifuna et al. 2019). Artesunate on the other hand, promotes heme alkylation through its 1,2,3-trioxane entity which implies that development of resistance to this novel hybrid might be delayed or altogether circumvented (Coslédan et al. 2008).

Absorption of drugs into blood systems depends on apical-basolateral (A-B) permeability. Since the intestinal membrane acts as the first barrier to orally administered large and charged molecules (Gessner and Neundorf 2020), poor performance and low drug concentrations at target regions is attributed to limited solubility in aqueous media (Mehmood et al. 2020).

A drug penetrates membranes through passive diffusion, active transport and paracellular transport (Knöpfel et al. 2019) and various *in silico* tools are available to calculate percentage HIA as a sum of bioavailability and absorption. HIA is evaluated from the ratio of excretion or cumulative excretion in urine, bile and feces (Zhao et al. 2002) and permeability of a compound to either Caco-2 cells or MDCK cells. MDCK cells predict oral drug absorption with high accuracy. Caco-2 cells have multiple transport channels through the intestinal epithelia that mimics most transport pathways in gastrointestinal tracts. ATSA exhibited a high percentage HIA of 96.83% and a Caco-2 permeability of 29.86 cm/sec compared to 88.675981% and 13.1902 cm/s respectively for ATS. ATSA has remarkably low MDCK cell permeability of 0.0695573 cm/sec compared to the 0.344241 cm/s for ATS. This suggests that ATSA is highly bioavailable to suppress malaria infections.

Drug delivery into blood circulation through the skin has a wide range of advantages such as stomach bypass, higher patient compliancy, expeditious delivery of drugs with short half-life or narrow therapeutic index among others (Parhi and Mandru 2021). Skin permeability index analysis for a new drug is thus important as it indicates whether across-the-skin delivery is possible. It also indicates the possible extent of damage due to accidental contact with a drug (Silva et al. 2014). A negative value for skin permeability of − 2.44849 (cm/h) for ATSA and − 3.77087 (cm/h) of ATS suggest that ATSA cannot penetrate the skin and thus is equally safe as artesunate.

Distribution of a drug is determined by calculating the BBB penetration and percentage PPB profiles. BBB is a ratio of drug concentration in the brain to its concentration in blood (C_{brain}/C_{blood}). Plasma protein binding of a drug influences its action and disposition as only unbound drug molecules are free to cross membranes by diffusion or active transport as well as for interaction with drug targets (Dohutia et al. 2017). From the results, ATSA has a considerably higher predicted BBB value of 0.355308 compared to 0.0112762 of ATS. It also has a higher PPB of 91.507% compared to 70.122% of ATS. A high BBB value may suggest that ATSA could find value in treatment of cerebral malaria. ATSA's high PPB is likely to modify its pharmacokinetics hence its bioavailability and efficacy.

Drug metabolism is key to its eventual excretion from the body. In this study, the Pre-ADMET tool analyzed whether ATSA is a substrate or an inhibitor to the members of the CYP subfamily: CYP 2C19 inhibition, CYP 2C9 inhibition, CYP 2D6 inhibition, CYP 3A4 inhibition, CYP 2D6 substrate and CYP 3A4 substrate. Our results (Table 2) show ATSA as an inhibitor of CYP 2C19, CYP 2C9, and CYP 3A4 genes and a non-substrate to CYP 2D6 genes. It inhibits CYP 2D6 but it is a substrate for CYP 3A4. This displays an additional safety of ATSA to the human host cells.

Ames mutagenicity, carcinogenicity, and hERG K^+ channel inhibition assays are used to determine toxicity profiles of drug candidates (Khan et al. 2017). Two strains of *Salmonella typhimurium*, TA100 and TA1535 (+ S9 activated with 10% liver homogenate and -S9 not activated) having mutations in genes responsible for histidine metabolism were used in predicting Ames test. The Ames test shows that ATSA is none mutagenic to the TA100 strain of bacteria. The hERG K^+ channels are predominately expressed in cardiac muscles and blockade of these channels by drugs induces acquired long QT syndrome that may trigger arrhythmias (Tschirhart et al. 2019). ATSA exhibit medium risks to hERG K^+ channel inhibition suggesting that it is safe.

Conclusion

Artesunate-3-chloro-4-(4-chlorophenoxy) aniline (ATSA) shows antimalarial chemosuppression activity against both the sensitive and the resistant human and mice malaria parasites with wide safety margins. This compound is thus a promising antimalarial drug candidate. To confirm the predicted ADMET parameters, in vivo studies are recommended. Pre-clinical and clinical studies should then follow to evaluate their value in the development of novel antimalarial drugs for future use in the management of multi-drug resistant malaria parasites.

Acknowledgements The authors would like to acknowledge Stephen Kaniaru of KEMRI-CBRD for his guidance during in vitro work and Mr. Lucas Ogutu of KEMRI animal house for providing mice for in vivo assays.

Author contribution Milka W. Waithera sourced for research funds and performed the experiments. Milka W. Waithera and Martin W. Sifuna analyzed data, drafted and revised the final manuscript. Daniel W. Kariuki, Johnson K. Kinyua, Francis T. Kimani, Joseph K. Nganga, and Masahiro Takei reviewed the final manuscript before submission.

Funding This study was funded by research grants from AFRICA ai JAPAN PROJECT (Innovation Centre for Molecular Biology and Biochemistry) 2014 and National Commission for Science, Technology and Innovation (NACOSTI/RCD/ST&I 6th CALL MSc 055) awarded to Milka Wambui Waithera.

Data availability The datasets generated and/or analyzed during the current study are available from corresponding author on reasonable request.

Declarations

Ethics approval and consent to participate The study was approved by KEMRI's ACUC, KEMRI-ACU 01/10/2018.

Consent for publication Not applicable.

Competing interests The authors declare no competing interests.

References

Angrisano F, Robinson LJ (2022) *Plasmodium vivax*-how hidden reservoirs hinder global malaria elimination. Par Int 87:102526. https://doi.org/10.1016/j.parint.2021.102526

Beteck RM, Smit FJ, Haynes RK, N'Da DD (2014) Recent progress in the development of anti-malarial quinolones. Mal J 13(1):1–10

Coslédan F, Fraisse L, Pellet A, Guillouc F, Mordmullerd B, Kremsnerd GP, Morenf A, Mazierf D, Maffrand J, Meunier B (2008) Selection of a trioxaquine as an antimalarial drug candidate. PNAS 105(45):17579–17584

Cravo P (2022) On the contribution of the rodent model *Plasmodium chabaudi* for understanding the genetics of drug resistance in malaria. Par Int 91:102623. https://doi.org/10.1016/j.parint.2022.102623

Dambuza NS, Smith P, Evans A, Norman J, Taylor D, Andayi A, Egan T, Chibale K, Wiesner L (2015) Antiplasmodial activity, *in vivo* pharmacokinetics and anti-malarial efficacy evaluation of hydroxypyridinone hybrids in a mouse model. Mal J 14(1):1–8

Dhanawat M, Das N, Nagarwal RC, Shrivastava SK (2009) Antimalarial drug development: past to present scenario. Mini-Rev Med Chem 9(12):1447–1469

Dohutia C, Chetia D, Gogoi K, Bhattacharyya DR, Sarma K (2017) Molecular docking, synthesis and *in vitro* antimalarial evaluation of certain novel curcumin analogues. Braz J Pharm Sci 53(4):1–14

Feng LS, Xu Z, Chang L, Li C, Yan X, Gao C, Ding C, Zhao F, Shi F, Wu X (2020) hybrid molecules with potential *in vitro* antiplasmodial and *in vivo* antimalarial activity against drug-resistant *Plasmodium falciparum*. Med Res Rev 40(3):931–971

Gessner I, Neundorf I (2020) Nanoparticles modified with cell-penetrating peptides: conjugation mechanisms, physicochemical properties, and application in cancer diagnosis and therapy. Int J Mol Sci 21(7):1–21

Hermansyah B, Fitri LE, Sardjono TW, Endharti AT, Arifin S, Budiarti N, Candradikusuma D, Sulistyaningsih E, Berens-Riha N (2017) Clinical features of severe malaria: protective effect of mixed plasmodial malaria. Asian Pac J Trop Biomed 7(1):4–9

Horata N, Choowongkomon K, Ratanabunyong S, Tongshoob J, Khusmith S (2017) Acquisition of naturally acquired antibody response to *Plasmodium falciparum* erythrocyte membrane protein 1-dblα and differential regulation of igg subclasses in severe and uncomplicated malaria. Asian Pac J Trop Biomed 7(12):1055–1061. https://doi.org/10.1016/j.apjtb.2017.09.017

Jonsson M, Jestoi M, Nathanail AV, Kokkonen UM, Anttila M, Koivisto P, Karhunen P, Peltonen K (2013) Application of OECD Guideline 423 in assessing the acute oral toxicity of moniliformin. Food Chem Toxicol 53(2013):27–32

Joseph H, Eriksson E, Schofield L (2019) Early suppression of B cell immune responses by low doses of chloroquine and pyrimethamine: implications for studying immunity in malaria. Par Res 118(6):1987–1992

Khan FM, Bari MA, Islam MK, Islam MD, Kayser MS, Nahar N, Faruk MA, Rashid MA (2017) The natural anti-tubercular agents: *in silico* study of physicochemical, pharmacokinetic and toxicological properties. J App Pharm Sci 7(5):34–38

Knöpfel T, Himmerkus N, Günzel D, Bleich M, Hernando N, Wagner CA (2019) Paracellular transport of phosphate along the intestine. Am J Physi-Gastro Liver Physi 317(2):G233–G241

Lombard M, N'Da DD, Van Ba CT, Wein S, Norman J, Weisner L, Vial H (2013) Potent in vivo anti-malarial activity and representative snapshot pharmacokinetic evaluation of artemisinin-quinoline hybrids. Mal J 12(1):1–7

Manohar S, Rajesh CU, Khan SI, Tekwani BL, Rawat DS (2012) Novel 4-aminoquinoline-pyrimidine based hybrids with improved *in vitro* and *in vivo* antimalarial activity. ACS Med Chem Let 3(3):555–559

Mehmood Y, Khan IU, Shahzad Y, Khan RU, Igbal MS, Khan HA, Yousaf AM, Khalid SH, Asghar S, Asif M, Hussain T, Shah SU (2020) In vitro and in vivo evaluation of velpatasvir-loaded mesoporous silica scaffolds. A prospective carrier for drug bioavailability enhancement. Pharmaceutics 12(307):1–18

Meunier B (2008) Hybrid molecules with a dual mode of action: dream or reality. Acco Chemi Res 41(1):69–77

Mosmann T (1983) Rapid colorimetric assay for cellular growth and survival: application to proliferation and cytotoxicity assays. J Immu Meth 65(80):55–63

Muller PY, Milton MN (2012) The determination and interpretation of the therapeutic index in drug development. Nat Re Drug Disc 11(10):751–761

Muregi FW, Ishih A (2010) Next-generation antimalarial drugs: hybrid molecules as a new strategy in drug design. Drug Dev Res 71(1):20–32

Nghochuzie NN, Olwal CO, Uduokang AJ, Amang-Etego LN, Amambua-Ngwa A (2020) Pausing the fight against malaria to combat the COVID-19 pandemic in Africa: is the future of malaria bleak? Fron Microbiol 11:1–5

Nilsen A, Miley GP, Forquer IP, Mather MW, Katneni K, Li Y, Pou S, Pershing AM, Stickles AM, Ryan E, Kelly JX, Doggett JS, White KL, Hinrichs DJ, Winter RW, Charman SA, Zakharov LN, Bathurst I, Burrows JN, Vaidya AB, Riscoe MK (2014) Discovery, synthesis, and optimization of antimalarial 4(1 H)-quinolone-3-diarylethers. J Med Chem 57(9):3818–3834

Odhiambo OC, Wamakima HN, Magoma GN, Kirira PG, Malala BJ, Kimani FT, Muregi FW (2017) Efficacy and safety evaluation of a novel trioxaquine in the management of cerebral malaria in a mouse model. Mal J 16(1):1–9

Omwoyo WN, Ogutu B, Oloo F, Swai H, Kalombo L, Melariri P, Mahanga GM, Gathirwa JW (2014) Preparation, characterization, and optimization of primaquine-loaded solid lipid nanoparticles. Int J Nanomed 9(1):3865–3874

Parhi R, Mandru A (2021) Enhancement of skin permeability with thermal ablation techniques: concept to commercial products. Drug Deliv Trans Res 11(3):817–841

Peters W, Portus JH, Robinson BL (1975) The chemotherapy of rodent malaria, XXII. Ann Trop Med Paras 69(2):155–171. https://doi.org/10.1080/00034983.1975.11686997

Sharma M, Chauhan K, Srivastava RK, Singh SV, Srivastava K, Saxena JK, Puri SK, Chauhan MS (2014) Design and synthesis of a new class of 4-aminoquinolinyl- and 9-anilinoacridinyl schiff base hydrazones as potent antimalarial agents. Chem Biol Drug Des 84(2):175–181

Sifuna MW, Wambui M, Nganga JK, Kariuki DW, Kimani FT, Muregi FW (2019) Antiplasmodial activity assay of 3-Chloro-4-(4-Chlorophenoxy) aniline combinations with artesunate or chloroquine in vitro and in a mouse model. BioMed Res Int 2019:1–7

Silva NSR, Gonçalves LKS, Duarte JL, Silva JS, Santos CF, Braga FS, Silva RC, Costa JS, Hage-Melim LIS, Dos Santos CBR (2014) Computational analysis of physicochemical, pharmacokinetic and toxicological properties of deoxyhypusine synthase inhibitors with antimalarial activity. Comp Mol Biosci 04(04):47–57

Tachibana M, Takashima E, Morita M, Sattabongkot J, Ishino T, Culleton R, Torii M, Tsuboi T (2022) *Plasmodium vivax* transmission-blocking vaccines: progress, challenges and innovation. Par Int 87(2021):102525. https://doi.org/10.1016/j.parint.2021.102525

Trager W, Jensen BJ (1976) Human malaria parasites in continous culture. Reports 193(4254):673–75

Tschirhart JN, Li W, Guo J, Zhang S (2019) Blockade of the human ether a-go-go–related gene (hERG) potassium channel. Mol Pharm 95(4):386–397

Varotti FDP, Botelho ACC, Andrade AA, Paula RC, Fagundes EMS, Valverde A, Mayer LMU, Mendonca JS, Souza MVN, Boechat N, Krettli AU (2008) Synthesis, antimalarial activity, and intracellular targets of mefas, a new hybrid compound derived from mefloquine and artesunate. Antimic Agents Chem 52(11):3868–3874

Zhao YH, Le J, Abraham MH, Hersey A, Eddershaw PJ, Luscombe CN, Boutina D, Beck G, Brad S, Cooper I, Platts JA (2002) Evaluation of human intestinal absorption data and subsequent derivation of a quantitative structure-activity relationship (QSAR) with the Abraham descriptors. J Pharm Sci 91(2):605